Геология и геофизика, *2023, т. 64, № 1, с. 150–160*, doi: 10.15372/GiG2022152
Поступила в редакцию 12.05.2021, принята в печать 13.09.2021

УДК 552.54+539.217.1(81)

ОЦЕНКА РАЗМЕРНОСТИ И ТИПА ПОРИСТОСТИ В АЛЬБСКОМ КАРБОНАТНОМ КОЛЛЕКТОРЕ БАССЕЙНА КАМПОС (*Юго-Восточная Бразилия*)

А.Г. Карраскилья, К. де Абреу

Laboratory of Engineering and Exploration of Petroleum (LENEP), Darcy Ribeiro Northern Rio de Janeiro State University, Amaral Peixoto Highway, Km 163, Brennand Avenue, S/N, Imboacica, Macaé, RJ, 27925310, Brazil

Альбские карбонаты свиты Киссама в бассейне Кампос на юго-востоке Бразилии являются важными коллекторами нефти. Они являются частью карбонатной платформы, которая сформировалась вдоль восточного побережья Бразилии и западного побережья Африки в альбе, что привело к открытию южной части Атлантического океана. Впоследствии карбонатный коллектор подвергся различным постседиментационным диагенетическим процессам. В настоящем исследовании для оценки пористости этого коллектора использовались результаты ГИС, включая данные по его плотности, пористости по нейтронному каротажу и результаты акустического каротажа. Полученные оценки плохо согласуются с лабораторными измерениями пористости. Учитывая тот факт, что каротажные диаграммы были получены разными физическими методами, для дальнейших оценок были использованы множественная линейная регрессия и искусственная нейронная сеть с байесовским стохастическим подходом, что позволило оценить пористость более точно. Поскольку пористость является важным петрофизическим параметром для характеристики коллекторов, в дальнейшем её значения использовались для оценки проницаемости и водонасыщенности карбонатного коллектора с помощью эмпирических уравнений. Недостаточно оценить лишь размерность пористости, необходимо еще и определить ее тип. Для этого были использованы пластовый коэффициент, коэффициент цементирования и значения извилистости поровых каналов и анизотропии. С их помощью были закартированы зоны первичной межзеренной и межчастичной пористости, а также вторичной пористости (разрывы, трещины и пустоты). Сделан вывод, что подобные исследования позволяют также выявить связанную и несообщающуюся пористости и, таким образом, оценить эффективную пористость вдоль скважины.

Бассейн Кампос, альбский карбонатный коллектор, оценка пористости, диаграммы ГИС

ESTIMATION OF THE SIZE AND TYPE OF POROSITY IN AN ALBIAN CARBONATE RESERVOIR OF THE CAMPOS BASIN, SOUTHEASTERN BRAZIL

A.G. Carrasquilla, C. de Abreu

The Albian carbonates of the Quissama Formation in the Campos Basin, southeastern Brazil, are important oil reservoirs. They make part of a carbonate platform that formed along the eastern coast of Brazil and the western coast of Africa during the Albian, which resulted in the opening of the South Atlantic Ocean. Subsequently, this reservoir was subjected to different postdepositional diagenetic processes. The present study utilized geophysical well logs to estimate the porosity of this reservoir, based on density, neutron porosity, and sonic logs. The estimates do not show good results when compared with the laboratory measurements. Then, exploring the fact that these logs are obtained with different physical principles, a multiple linear regression and an artificial neural network with Bayesian stochastic approach were applied, which resulted in a better porosity estimate. As porosity is a petrophysical parameter considered significant in the characterization of reservoirs, it was used, hereafter, to estimate permeability and water saturation of the reservoir, applying empirical equations. From there, it was not enough just to estimate the porosity, but was necessary to know what type it is. For this purpose, the concepts of the electrical formation factor, cementation coefficient, tortuosity, and anisotropy were used. With them, the zones with primary intergranular and interparticle porosity as well as secondary porosity, such as fractures, fissures, and vugs, were mapped. It was concluded that, with studies of this type, it is also possible to identify the connected and nonconnected porosities, which permits estimation of the effective porosity along the well.

Campos Basin, Albian carbonate reservoir, porosity estimates, geophysical well logs

INTRODUCTION

The estimation of petrophysical parameters from log data is of supreme importance for evaluation of the quality of hydrocarbon reservoirs, identification of exploratory potential, and management of production wells. Porosity (ϕ) is the void or space inside the rock, which is especially useful for storing fluids; it is also useful in

✉e-mail: abel@lenep.uenf.br

the transmission of these fluids in the case of good permeability. In addition, other petrophysical parameters, such as permeability (k) and water saturation (S_w), are derived from its estimation through empirical relationships. The porosity cementation exponent (m), the connected (ϕ_c) and unconnected (ϕ_{nc}) porosity, the electrical formation factor (F), and the tortuosity coefficient (τ) can also be calculated from ϕ (Kennedy, 2015).

Direct measurements for determining ϕ are made in the laboratory using volumetric or petrographic analysis of small rock samples. Because of the expense of obtaining samples to measure ϕ, typically, only a few wells are cored. The wells that do get cored are usually appraisal wells, drilled early in the life of the reservoir, and key wells throughout the reservoir (Schön, 2011).

Indirect methods to estimate ϕ are commonly applied with geophysical well logs. Logs are routinely performed in wells, if only to identify the depths of the productive intervals. The three more common open-hole logs used to evaluate ϕ are sonic (*DT*), density (*RHOB*), and neutron (*NPHI*) logs. Other logs used to determine it include nuclear magnetic resonance (*NMR*) tools and the electromagnetic-propagation tool (*EPT*); however, they are not very frequent. Thus, ϕ estimation is an important step in the log analysis, and it could only be done correctly after a good lithology interpretation (Ellis and Singer, 2007).

Accurate determinations of petrophysical properties in carbonate reservoirs (i.e., ϕ, k, and S_w) require detailed knowledge of pore types. Traditional methods of estimating hydrocarbon reserves are also sensitive to variations of the pore types. Usually, *NPHI* and *RHOB* wireline logging devices are assumed to indicate total porosity (ϕ_t). However, in this study, the estimate that best fits the laboratory experimental porosity data (ϕ_{lab}) will be considered ϕ_t. In reservoirs in which moldic or separate (vug) porosity exists, a distinction between moldic and interparticle porosity is especially important for precise determination of petrophysical properties. Conventionally, a *DT* log is chosen to provide information on the volume of moldic porosity. However, as the *DT* tool is commonly considered to be of secondary importance, acoustic logs are uncommon in many datasets. Resistivity (*RT*) logs can also provide valuable information on the volume of moldic porosity in much the same way as sonic logs do. Accordingly, a well-constrained methodology for determining the moldic pore volume from *RT* logs offers great potential for improving the accuracy of reservoir-wide petrophysical calculations (Lucia, 1983).

GEOLOGIC CONTEXT

The Campos Basin is limited to the north by the Espírito Santo Basin, through the Vitória Arch, and to the south, by the Santos Basin, through the Cabo Frio High. It occupies an area of about 115,800 km^2, of which only 500 km^2 are not immersed (Fig. 1). Its origin is related to the rupture of the Gondwana Supercontinent, which started from the Lower Cretaceous. The regional tectonostratigraphic evolution is divided into three supersequences, called Rift, Postrift, and Drift (Bruhn et al., 2003).

The Albian Quissamã Formation, the focus of studies of this work, is included in the Drift supersequence; it corresponds to the free marine stage of the Campos Basin, which was deposited between lower and middle Albian, corresponding to the basal portion of the Macaé Group. It consists of a thick carbonate section that reaches 800 m in some portions of the basin. Lithologically, oolitic, oncolitic, and peloidal calcarenites and calcirrudites predominate, with increasing intercalations of calcisiltites, calcilutites, and marl toward the top. The base of this unit, in the south and central regions of the basin, is generally dolomitized, being called the Búzios Member. The lower limit of the Quissamã Formation corresponds to a discordant surface, with abrupt contact between the Albian carbonates and the evaporitic deposits of the Retiro Formation, of Aptian age. The upper limit is equivalent to a maximum flood surface, expressed in regional stratigraphic landmarks called Beta and Glauconitic; the proximal portion is dated from the Mesoalbian. Capping the Quissamã Formation, the Outeiro Formation is composed of calcilutites, notably bioclastic mudstones rich in microfossils, and intercalations of marl and shales, reaching 300 m in thickness. The depositional model referring to the Quissamã Formation includes, on the southwest margin of the basin, lagoonal and beach environments, which gradually evolved into a regional carbonate platform, with elongated oolithic benches in the NE–SW direction. The depositional geomorphology would be that of a carbonate ramp, with a low dip in an east–northeast direction, strongly affected by halokinetic movements from the Eo-Mesoalbian limit (Fig. 2). This adiastrophic tectonics influences the substrate morphology, leading to the formation of low deposits and high areas, which control the faciological variation observed throughout the Quissamã Formation (Okubo et al., 2015).

MATERIALS AND METHODS

In the studied oil field of this basin, named Oil Field B, one existing well was selected to carry out this research for having a better dataset. Well B17 has a dataset formed by the basic suite of geophysical well logs, with gamma ray (*GR*), *RT*, *NPHI*, *RHOB*, and sonic *DT* along with lithological and petrophysical laboratory measurements.

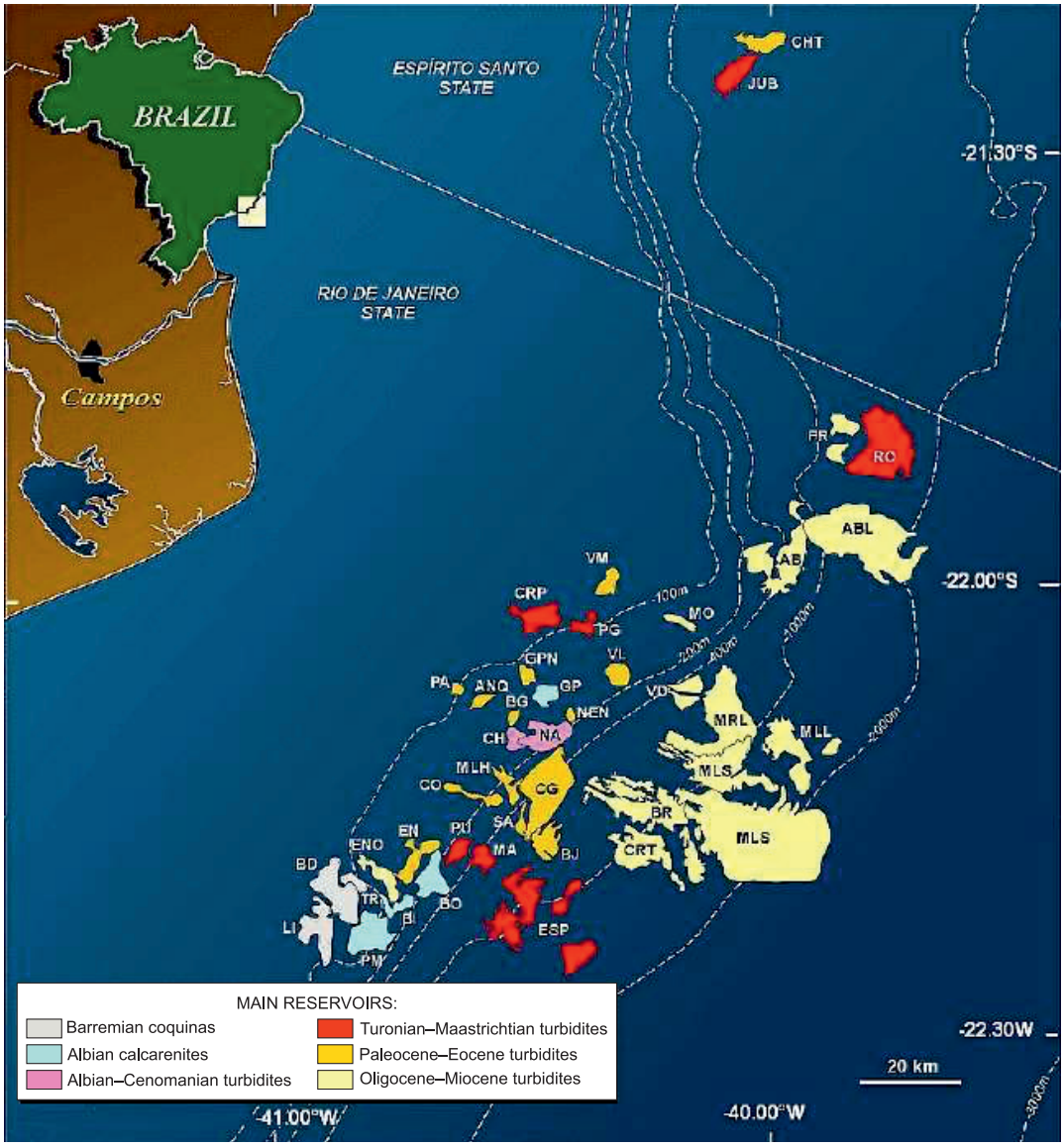

Fig. 1. Location of the main oil fields of the Campos Basin. The red dashed rectangle shows the oil field considered in this study.

Oil fields: GP, Garoupa; PG, Pargo; GPN, Garoupinha; BG, Bagre; NA, Namorado; BD, Badejo; CH, Cherne; EN, Enchova; BI, Bicudo; PM, Pampo; BO, Bonito; LI, Linguado; CO, Corvina; VL, Viola; PA, Parati; CG, Congro; PU, Piraúna; ENO, Enchova Oeste; ANQ, Anequim; CRP, Carapeba; TR, Trilha; VM, Vermelho; MO, Moréia; MA, Marimbá; AB, Albacora; MRL, Marlim; MLH, Malhado; ABL, Albacora Leste; FR, Frade; MLL, Marlim Leste; VD, Voador; NEN, Nordeste de Namorado; MLS, Marlim Sul; ESP, Espadarte; BR, Barracuda; BIJ, Bijupirá; SA, Salema; CRT, Caratinga; RO, Roncador; JUB, Jubarte; CHT, Cachalote (modified from (Bruhn et al., 2003)).

Initially, the logs were plotted, interpreted qualitatively, and compared with the available lithology. Then, the porosity was estimated using *NPHI*, *RHOB*, and *DT* logs individually. Among these logs, only the *NPHI* log directly measures porosity, while *RHOB* and *DT* estimate this parameter based on theoretical or empirical considerations. The measurements obtained from them are not only dependent on the porosity but are also dependent on other rock properties, such as lithology (rock type: sandstone, limestone, shale, etc.), the fluids occupying the pore spaces, the wellbore environment (type of drilling fluid and hole size), and the geometry of the pores. Since many variables may impact the log readings, corrections need to be applied to the log interpretations and the three logs are typically evaluated together to determine the best estimate of the porosity of rock formations. The log evaluations are also calibrated against sample porosity in wells where cores, plugs, and logs are available. Thus, this joint analysis of porosities provides a perspective to understand the distortions between them. These biases might come from the different physical approaches on which each log is based to estimate

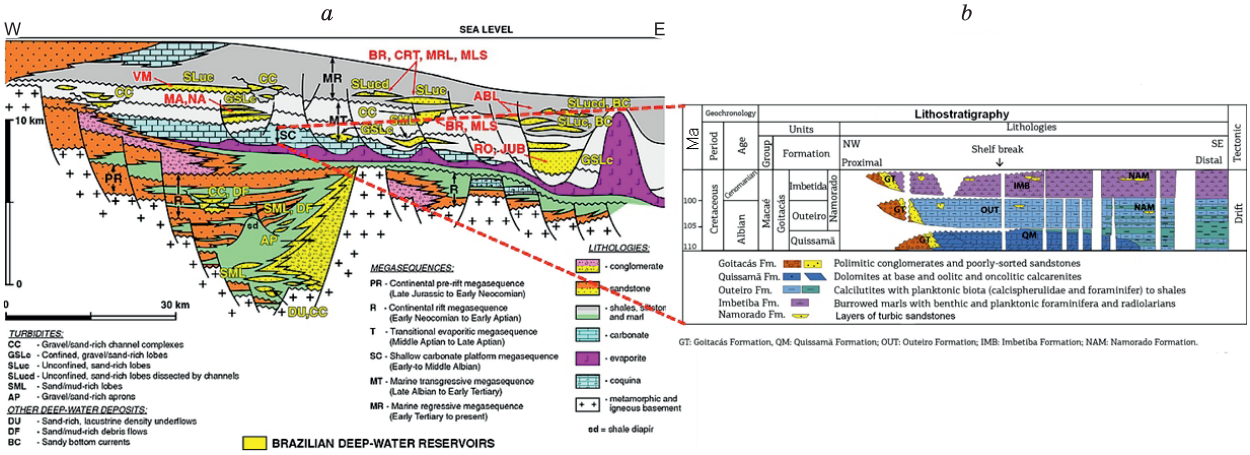

Fig. 2. *a*, Generalized geologic section for the Eastern Brazilian continent-marginal basins.

The main megasequences are PR, prerift (which does not occur in the Campos Basin); R, rift; T, transitional (which includes the evaporate section); SC, shallow carbonate; MT, marine transgressive; and MR, marine regressive; *b*, zoom of the stratigraphy of the postsalt carbonates of the Campos Basin, emphasizing the studied portion, the dolomites and the calcarenites of the Quissamã Formation (QM) (modified from (Okubo et al., 2015)).

porosity. The porosity of a zone can be estimated either from a single "porosity log" or a combination of porosity logs to correct for variable lithology effects in complex reservoirs. It can be seen that the physical principles of each log used to estimate porosity are different and interact differently with the geologic formation. Thus, a combination of these logs could be useful to estimate porosity, because it gives good indications for lithology and more accurate estimates of porosity, which is one of the main objectives of this study (Luthi, 2001).

For instance, an *NPHI* log measures the amount of hydrogen in the formation being logged, emitting neutrons from a chemical or electronic source, which collide with the nuclei of elements in the formation. Thus, the neutron porosity (ϕ_{NPHI}) is estimated using the following equation:

$$\phi_{NPHI} = \sum_{1}^{n} V_i \, \phi_{aapi} \approx \sum_{i=1}^{n} V_i I_{HI} \,, \tag{1}$$

where ϕ_{NPHI} is the response of the neutron log (*pu*, porosity units); V_i is the fractional volume of each mineral or fluid (fraction); ϕ_{aapi} is the apparent neutron porosity (*pu*, porosity units); and I_{Hi} is the hydrogen index (Schlumberger, 1989).

The *DT* log measures the acoustic transit time in the formation, and *DT* porosity (ϕ_{DT}) obtained from this log is expressed by the equation of Wyllie et al. (1956):

$$\phi_{DT} = \frac{\Delta t_{log} - \Delta t_{ma}}{\Delta t_f - \Delta t_{ma}} \,, \tag{2}$$

where Δt_{log} is the *DT* log (μs/m); Δt_{ma} is the transit time in the rock matrix (μs/m); and Δt_f is the transit time of fluids in rock pores (μs/m).

The *RHOB* log, meanwhile, measures the electron density of the formation emitting gamma rays from a chemical source, which interact with the electrons of elements in the formation. The expression for ϕ_{RHOB}, the porosity derived from the *RHOB* log, is also derived from (Wyllie et al., 1956):

$$\phi_{RHOB} = \frac{\delta_{log} - \delta_{ma}}{\delta_f - \delta_{ma}} \,, \tag{3}$$

where δ_{log} is the measured log density (g/cm^3); δ_{ma} is the density of the rock matrix (g/cm^3); and δ_f is the fluid density (g/cm^3), generally equal to that of the formation water (1.2 g/cm^3).

As emphasized above, if the individual ϕ estimates do not work, there is the alternative of making a joint estimate of them, exploring the fact that they come from different physical principles. To do this, initially, we propose a multiple linear regression (*MLR*), the goal of which is to model the linear relationship between the independent variables (ϕ_{NPHI}, ϕ_{RHOB}, and ϕ_{DT}) and response variable (ϕ_{MLR}). The process is conducted using an

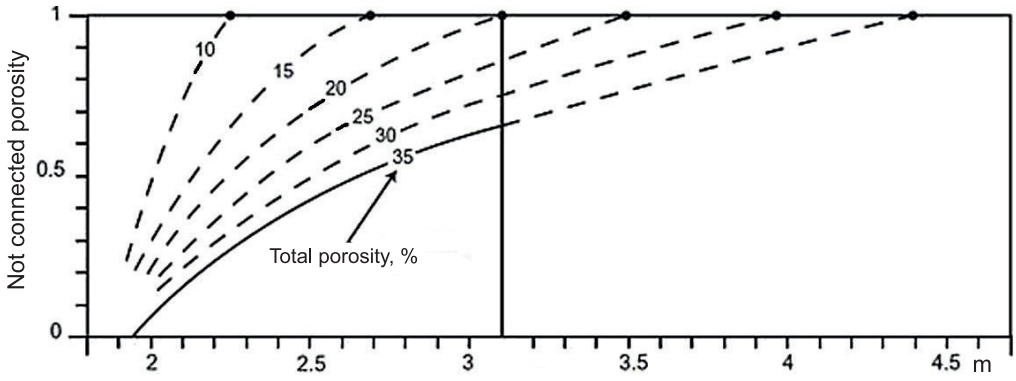

Fig. 3. Relationship between unconnected porosity and Archie's cementation coefficient (adapted from (Focke and Munn, 1987)).

inverse algorithm that employs the Levenberg–Marquardt approach, which is applied to solving nonlinear least-squares forward problems (Olive, 2017). Still, if this approach does not go well, it is proposed to use a nonlinear stochastic approach in the direction of artificial neural networks. For this, the approach of Bayesian regularized artificial neural networks is proposed, which is a mathematical process that converts a nonlinear regression into a "well-posed" statistical problem in the manner of a ridge regression. In this case, the input of the algorithm would be ϕ_{NPHI}, ϕ_{RHOB}, and ϕ_{DT}, and the output would be ϕ_{ANN} (Burden and Winkler, 2008).

Archie (1942) developed his famous equation to calculate, from well log parameters, S_w of the uninvaded zone in a formation next to a borehole:

$$S_w^n = \frac{R_w}{\left(\phi_t^m R_t\right)}, \tag{4}$$

where S_w is the water saturation of the uninvaded zone (%); n, saturation exponent; R_w, formation water resistivity at formation temperature (Ohm·m); ϕ_t, total porosity (%); m, cementation exponent; and R_t, true resistivity (Ohm·m). Fortunately, n does not change much, between 1.5 to 2.5. However, as shown in Fig. 3, m commonly takes values that change between 1.9 to 4.4 when unconnected porosity (ϕ_{nc}) increases within the same total (ϕ_t) and connected (ϕ_c) porosity, while $\phi_t = \phi_c + \phi_{nc}$ (Serra and Serra, 2004).

In his experiments, Archie (1942) began with naming the ratio of the resistivity of the fully water-saturated rock sample (Ohm·m) (ρ_o) to the resistivity of the water saturating the pores (Ohm·m) (ρ_w) the resistivity formation factor F. It depends also on ϕ in the form of an inverse power law of m, as it appears in the second factor of Eq. 5, but the equation can be arranged as it appears in the last factor:

$$F = \frac{\rho_o}{\rho_w} = \phi_t^{-m} = \phi_t^{-1}\phi_t^{1-m}, \tag{5}$$

where ρ_o, ρ_w, m, and ϕ_t are as explained before. Archie (1942), Glover (2009, 2016), Ellis and Singer (2007), Gartner and Suau (1980), Lucia (1983), Ahr (2011), and Focke and Munn (1987) made extensive analyses in their studies in relation to the values of F and m in different rock conditions of porosity and fluids.

The secondary porosity partition by the DT log has been widely used to estimate the apparent porosity exponent by applying the Nugent equation, which has the form of the first factor of Eq. 6 and, by replacing the ϕ_{DT} by the ϕ_c estimate, we obtain a modification of this equation, as it appears in the second factor (Tiab and Donaldson, 2012):

$$m_a = -\frac{2\cdot\log\left(\phi_{DT}\right)}{\log\left(\phi_t\right)} = -\frac{2\cdot\log\left(\phi_c\right)}{\log\left(\phi_t\right)}, \tag{6}$$

where m_a is the apparent porosity exponent and ϕ_{DT}, ϕ_c, and ϕ_t are as explained above. The DT log could be related to ϕ_{nc} by

$$\phi_{nc} = \left(\frac{\phi_t - \phi_{DT}}{1 - \phi_t}\right), \tag{7}$$

which simply represents a rescaling of the secondary porosity to the matrix volume rather than to the bulk volume, while ϕ_c is then (Doveton, 2014)

$$\phi_c = \left(\frac{\phi_{DT} - \phi_t^2}{1 - \phi_t} \right). \tag{8}$$

However, there exists another useful parameter related to F, electrical tortuosity (τ). It is a ratio that characterizes the convoluted pathways of electrical conduction through porous media, which is often written as in the first factor of Eq. 9, but it can also be expressed as in the second factor of this equation (Wyllie, 1957):

$$\tau = F\phi_t = \phi_t^{1-m}. \tag{9}$$

Essentially, τ measures the path sinuosity inside connected pores of the rock, and it is a petrophysical parameter that can be related to the rock permeability (Ahr, 2011).

As laboratory permeability experimental data exist in the dataset in the form of total (k_t), horizontal (k_h), and vertical (k_v) permeabilities, they were incorporated into this study as a complement to the previous porosity estimates. To do this, the permeability anisotropy (g) coefficient was calculated as the square root of the ratio between k_h and k_v (Sahin et al., 2007):

$$g = \sqrt{\frac{k_h}{k_v}}. \tag{10}$$

Finally, when good-quality core data are not available, k estimates can be made from empirical equations, which is controlled by factors, such as pore size and pore-throat geometry as well as porosity. To take some account of these factors, Timur (1968) developed an empirical equation to estimate *kt*:

$$k_t = \frac{10^a \phi_t^b}{S_{wirr}^c}, \tag{11}$$

where k_t is the total permeability (*mD*); ϕ_t is as defined above; S_{wirr} is the water saturation (*pu*); and $a = 4$, $b = 4.5$, and $c = 2$ are regression constants (Lucia, 1983). There exist different ways to estimate S_{wirr}, but in this work, it was estimated from an S_w vs. depth plot in the hydrocarbon-bearing zone. In this portion of the well, where there is the highest oil saturation and the minimum water saturation, this last one is S_{wirr} (Tiab and Donaldson, 2012).

RESULTS

Initially, a qualitative petrophysical analysis was performed for the geophysical logs of Well B17. Figure 4 shows, from left to right, the *GR* (track 1), *RT* (track 2), *NPHI* (track 3), *RHOB* (track 4), and *DT* (track 5) logs and the lithologic column (track 6) proposed by Petrobras (2012) for this well. Thus, the description, by depth range, is as follows:

– between 0 and 50 m depth, the *GR* log indicates high values (> 30° API), related to the presence of mudstone. The *RT* log shows low values (<20 Ohm·m); the *NPHI* log, porosity values with an average of 20%; the *RHOB* log, densities above 2.2 g/cm^3; and the *DT* log, average values of 250 μs/m. At a depth of 20 m, the high value that the *DT* log shows is notable (up to 420 μs/m), which may be related to the presence of fractures;

– between 50 and 90 m, the *GR* log shows low values (around 20° API), related to the presence of grainstones, packstones, and wackestones at these depths, which is the carbonate reservoir of this field. The *RT* log shows high values (between 20 and 1000 Ohm·m), mainly owing to the presence of hydrocarbons in the pores of this reservoir. The *NPHI* log is characterized by porosity values between 20 and 35%, showing an interval with good porosity, compatible with an Albian carbonate reservoir. The *RHOB* log shows densities around 2.2 g/cm^3, within the carbonate range (1.93–2.90 g/cm^3). Finally, the *DT* log is characterized by values above 250 μs/m;

– between 90 and 120 m, the *GR* log indicates values between 15 to 30° API, related to the presence of grainstones, packstones, and wackestones, but without reservoir characteristics. The *RT* log shows falling values, from 100 to less than 10 Ohm·m, indicating the presence of an aquifer horizon. The *NPHI* log is characterized by porosity values between 10 and 20%, showing a decrease in porosity in the aquifer. The *RHOB* log shows densities around 2.3 g/cm^3, again within the carbonate range. Finally, the *DT* log demonstrates ascending values from 250 to 300 μs/m;

– between 120 and 160 m, the *GR* log shows values between 15 to 30° API, related to the presence of mudstones. The *RT* log shows falling values, from 10 to 1 Ohm·m of a mudstone layer. The *NPHI* log is characterized by porosity values between 10 and 25%, demonstrating a rise in porosity in this layer. The *RHOB* log shows densities ranging from 2.3 to 2.5 g/cm^3. At a depth of 150 m, it is possible to observe low density, up to 1.7 g/cm^3, which can be attributed to the presence of vugular porosity or any problem in measuring the *RHOB* log. Finally, the *DT* log shows rise values from 190 to 280 μs/m.

Table 1. **Goodness of fit for porosity estimates**

Type of porosity	R^2	*RMSE*
ϕ_{NPHI}	0.21	21.08
ϕ_{RHOB}	0.07	0.09
ϕ_{DT}	0.32	0.07
ϕ_{MLR}	0.42	0.06
ϕ_{ANN}	0.65	0.02

After this examination, the porosities were estimated for Well B17 using *NPHI*, *RHOB*, and *DT*, along with the estimate that mixes these three through a multiple linear regression (*MLR*) and an artificial neural network (*ANN*) approach, which were plotting together with the laboratory porosity (ϕ_{lab}, in black dots) (Fig. 5). Tracks 1 to 5 show estimates for ϕ_{NPHI}, ϕ_{RHOB}, ϕ_{DT}, ϕ_{MLR}, and ϕ_{ANN}, respectively. As this figure shows, the fits between the first three estimates and ϕ_{lab} data are not particularly good. This is confirmed by the statistical analysis of the quality of these adjustments, as shown in Table 1. The ϕ_{RHOB} estimate is the worst, as it shows exceptionally low Pearson's determination coefficient $R^2 = 0.07$, but a good root mean square error *RMSE* = 0.09. Next, ϕ_{NPHI} has an $R^2 = 0.21$, better than ϕ_{RHOB}, but a high *RMSE* = 21.08. The ϕ_{DT} appears better than the previous two, with $R^2 = 0.32$ and *RMSE* = 0.07. The ϕ_{MLR} shows $R^2 = 0.42$ and *RMSE* = 0.06. The best estimate, however, is the ϕ_{ANN}, which presents $R^2 = 0.62$ and *RMSE* = 0.02. These results show that the porosity estimate improves when we mix these estimates made using different physical methods.

The coefficients of the *MLR* equation show a bigger positive contribution (0.78) of ϕ_{DT} in this estimate, with a negative contribution of ϕ_{NPHI} and ϕ_{RHOB}, with –0.0006 and –0.46, respectively (Eq. 12). This indicates that for the geologic structure found in this well, the *DT* log is a more appropriate estimate for porosity, which has already been shown in the values of R^2 and *RMSE* in Table 1.

$$\phi_{MLR} = 0.15 - 0.006\phi_{PHI} - 0.46\phi_{RHOB} + 0.78\phi_{DT}\,. \tag{12}$$

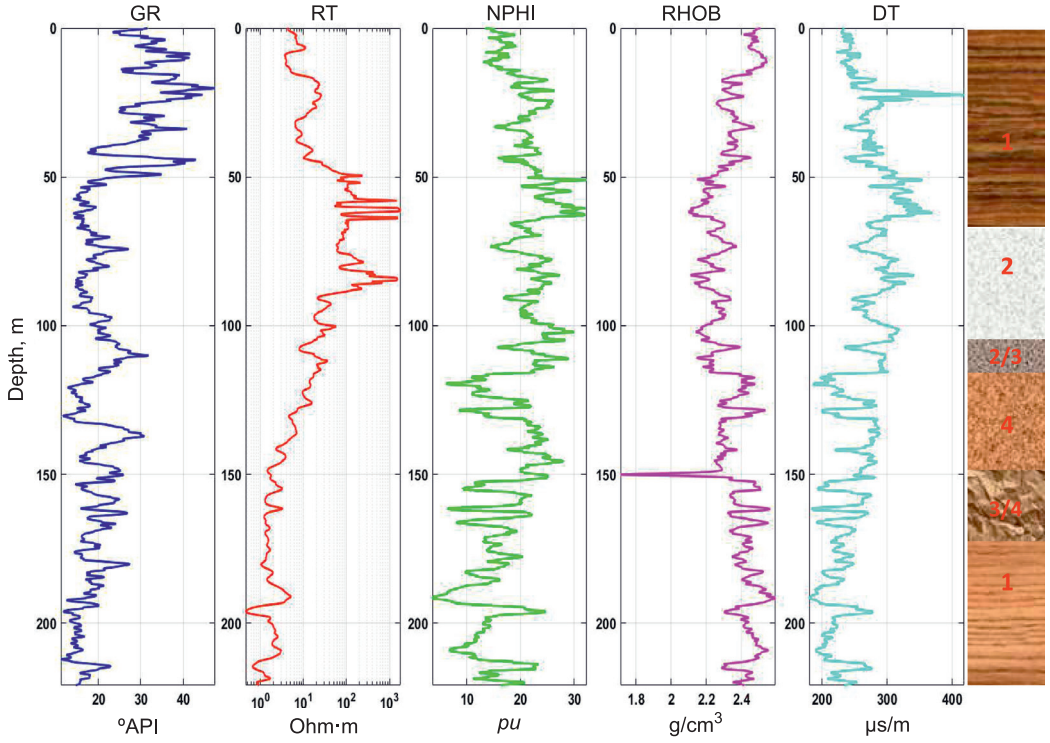

Fig. 4. Basic logs of Well B17: track 1, gamma ray (GR); track 2, resistivity (RT); track 3, neutron porosity (NPHI); track 4, density (RHOB); track 5, sonic or delay time (DT); track 6, lithologic section interpreted by Petrobras (2012). 1, Mudstone; 2, Grainstones; 3, Grainstones/Packstones; 4, Wakestones/Packstones.

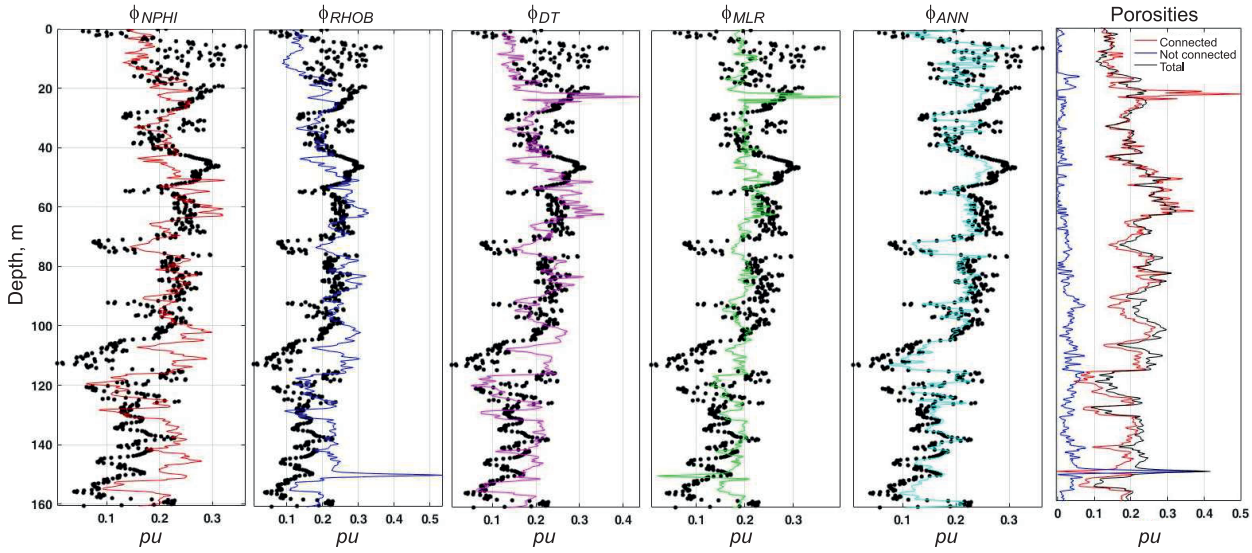

Fig. 5. Porosity estimates in Well B17: track 1, neutron porosity (ϕ_{NPHI}); track 2, density porosity (ϕ_{RHOB}); track 3, sonic porosity (ϕ_{DT}); track 4, multiple linear regression porosity (ϕ_{MLR}); track 5, artificial neural network porosity (ϕ_{ANN}); track 6, connected and unconnected porosities.

In the case of the *ANN* estimate, Eq. 13 shows the relationship found between ϕ_{ANN} and ϕ_{lab}, which resulted in $R^2 = 0.65$ and $RMSE = 0.02$, demonstrating a good improvement in relation to the *MLR* estimate (track 5):

$$\phi_{ANN} = 0.64\phi_{lab} + 0.069 . \quad (13)$$

In track 6 of Fig. 5, the connected (red curve, ϕ_c) and nonconnected (blue curve, ϕ_{nc}) porosities are plotted. As can be seen in this figure, ϕ_c is important throughout the reservoir, with values close to total porosity ϕ_{ANN} (black curve), around 30%. The ϕ_{nc} value is slightly larger at a depth of 20 m (5%), where there is sealing rock, and after 90 m (10%), where there is no reservoir. The peak at a depth of 150 m (up to 40%) is attributed to the presence of unconnected porosity (perhaps, vugs).

Having a more reliable estimate of the porosity, we proceed to estimate other petrophysical parameters, such as k_t and S_w. Thus, track 1 in Fig. 6 shows the ϕ_{ANN} (red curve) and ϕ_{lab} (black dots), and track 2 shows the permeability k_t estimated using the Timur approach (magenta curve) and plotted together with the permeability measured in the laboratory (k_{LAB}, blue dots). Finally, S_w estimated in Archie's equation using ϕ_{lab} (black dots) plotted together with S_w calculated with Archie's equation, but using ϕ_{ANN}. Table 2 helps us to analyze the quality of each adjustment. In the case of ϕ_{ANN}, the analysis is the one made above. In the case of k, Table 2 shows an $R^2 = 0.54$, worse than the porosity estimate, but a higher $RMSE = 3.34$. In the case of S_w, we see an excellent value for $R^2 = 0.97$ and a low $RMSE = 0.17$. This leads us to conclude that despite a not particularly good fit in the porosity, this bad estimate is not transmitted to the k_t and S_w cases.

Figure 7 presents the ϕ_{RHOB} vs. ϕ_{DT} cross-plot (*a*) and *m* and τ plots (*b*). In part *A*, according to Hakimi et al. (2012), number 1 shows the primary intergranular connected porosity, above the 45° line. Number 2 shows the secondary porosity, below the 45° line, with fractures, fissures, and unconnected microporosity. In part *B* of the same figure, the plots of Archie's parameters, *m* (left) and τ (right), are presented. According to Ohen et al. (2002), for $m = 1.4$, these are fractures (*a*); $m = 2.0$ is intergranular, intracrystalline, and/or interparticle porosity (*b*); $m \geq 2.3$ are vugs (*c*); and $m > 3$ is moldic porosity (*d*). The τ plot, meanwhile, demonstrates low values (<10) between the 20 and 110 m depths, which is where the reservoir is located, showing that the flow in this interval is less tortuous, which increases k_t. For depths less than 20 and greater than 120 m, the values are higher than 20, which indicates tortuous paths for the flow of liquids.

Finally, Fig. 8 shows the values measured in the laboratory, on samples, for k_h (track 1) and k_v (track 2). Tracks 3 and 4 show the permeability anisotropy coefficient (*g*) and the k_h vs. k_v cross-plot,

Table 2. **Goodness of fit for porosity, permeability, and water saturation estimates**

Parameter	R^2	*RMSE*
ϕ_{ANN}	0.65	0.02
k	0.54	3.34
S_w	0.97	0.17

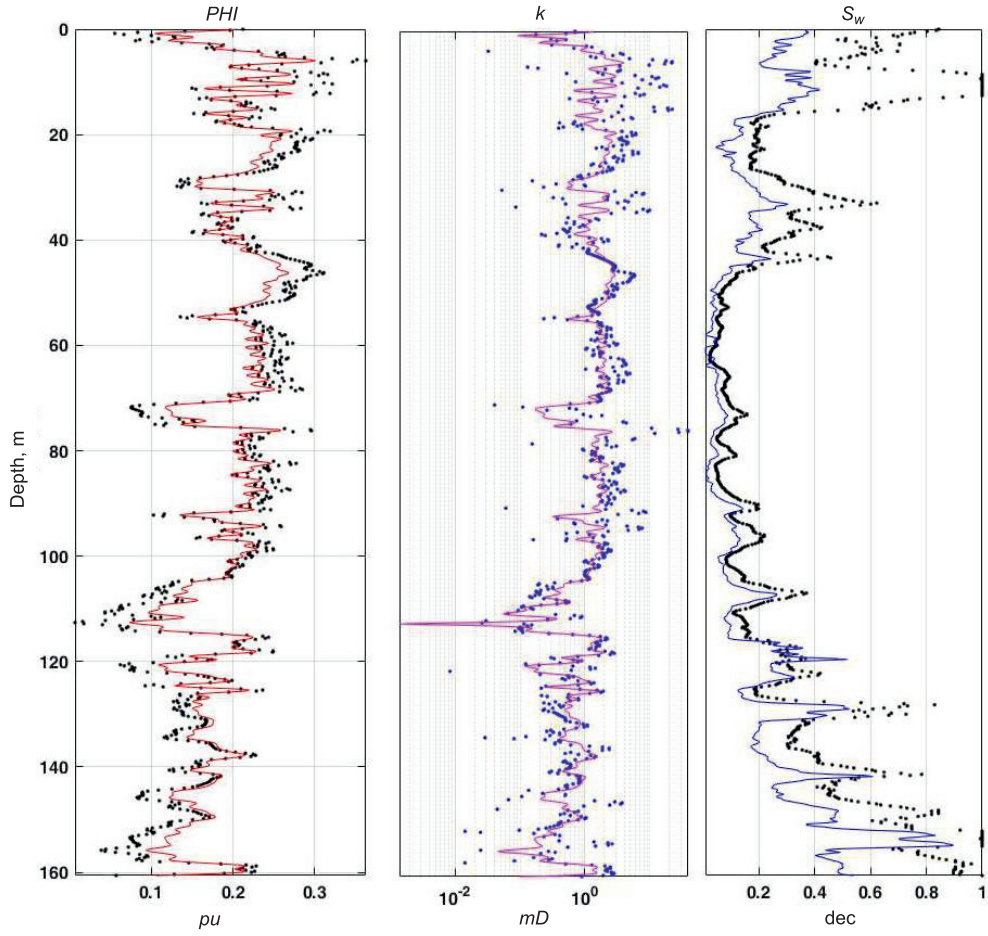

Fig. 6. Estimates of track 1, multiple linear regression porosity (ϕ_{MLR}); track 2, Timur's permeability (k_t); track 3, Archie's water saturation (S_w).

respectively. Between 50 and 100 m, k_h and k_v are remarkably similar, which is corroborated by the value $g = 1$ (that is, an isotropic geologic horizon) (track 3). This zone is precisely where the reservoir is located, highlighted by the grainstone lithology, which presents the best production rates. Anisotropic geologic media, with $1 < g < 1$ ($g \neq 1$), occur at depths outside the range mentioned before (track 3). The cross-plot of this figure illustrates that the biggest differences between the two permeabilities appear when the values are outside the 45° line, in the blue dots of the graph, precisely at low depths (track 4).

CONCLUSIONS

In this work, Well B17 of Oil Field B, Campos Basin, Southeastern Brazil, was selected to understand the porous system of the reservoir. This borehole was drilled through an Albian carbonate reservoir of the Quissamã Formation. In this reservoir, porosity was estimated in the traditional way, using the density, neutron porosity, and sonic geophysical well logs. This did not result in good estimates compared with the porosity measurements performed in the laboratory. Taking advantage of the fact that these estimates are made with logs that use different physical principles, a multiple linear regression that employs the Levenberg–Marquardt method and an artificial neural network with a Bayesian stochastic approach was performed with these porosities, which were better than the initial ones. After that, important petrophysical parameters, such as permeability and water saturation, were estimated using empirical equations. From that point, interest arose in estimating not simply the porosity size but also its type along the wellbore. For this purpose, concepts from Archie's equation were used, such as the electrical formation factor, cementation exponent, and tortuosity along with the permeability anisotropy coefficient. The results indicate that this reservoir has a complex geology and that it is not easy to estimate porosity through the logs. Even so, the criteria used to know the porosity type showed the areas with primary (intergranular and interparticle type) and secondary (fractures, fissures, and vugs) porosity. The

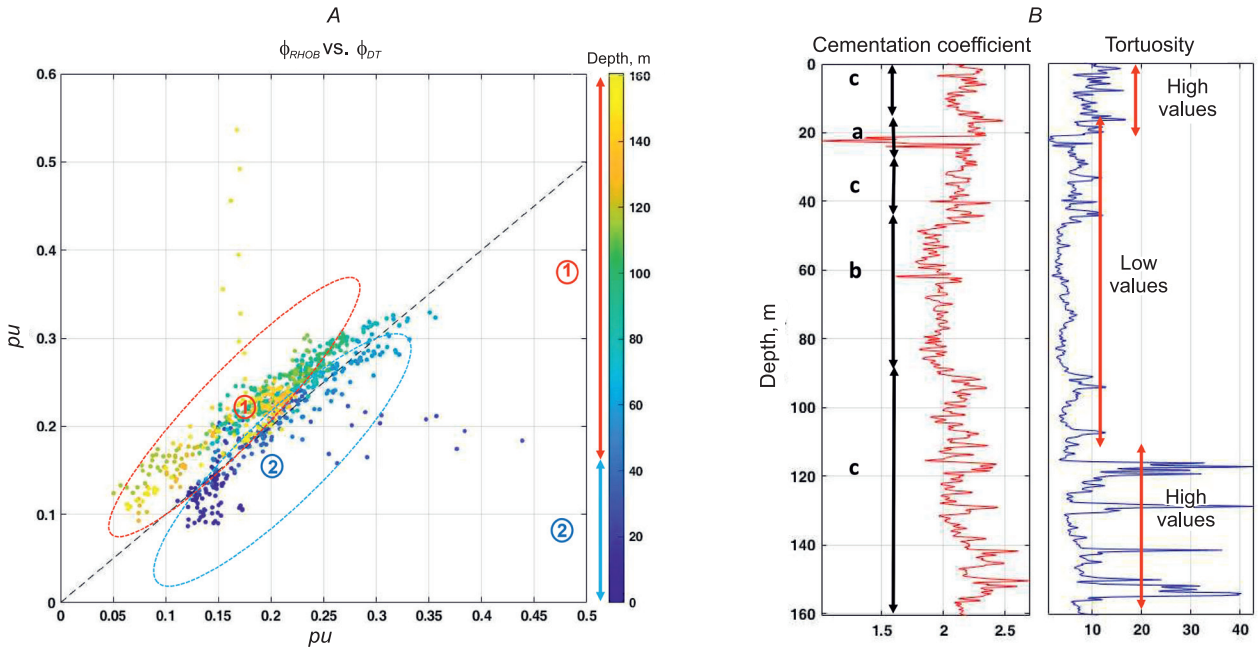

Fig. 7. *a*, Cross-plot ϕ_{RHOB} vs. ϕ_{DT}; *b*, *m* and τ plots vs. depths.

A, porosity: 1, primary porosity, intergranular connected, above the 45° line; 2, secondary porosity, fractures, fissures, micro porosity unconnected, below the 45° line (Hakimi et al., 2012). *B*, cementation coefficient: *a*, fractures, $m = 1.4$; *b*, intergranular/intercrystalline, $m = 2.0$; c, vugs, $m \geq 2.3$ (Ohen et al., 2002).

tortuosity values are lower in the areas of primary porosity and high in the areas of secondary porosity, demonstrating that a better flow exists at the depths with intergranular and interparticle porosity. Finally, the permeability anisotropy coefficient shows values close to 1 along the grainstone reservoir and higher values at the shallowest (<50 m) and greatest (>100 m) depths.

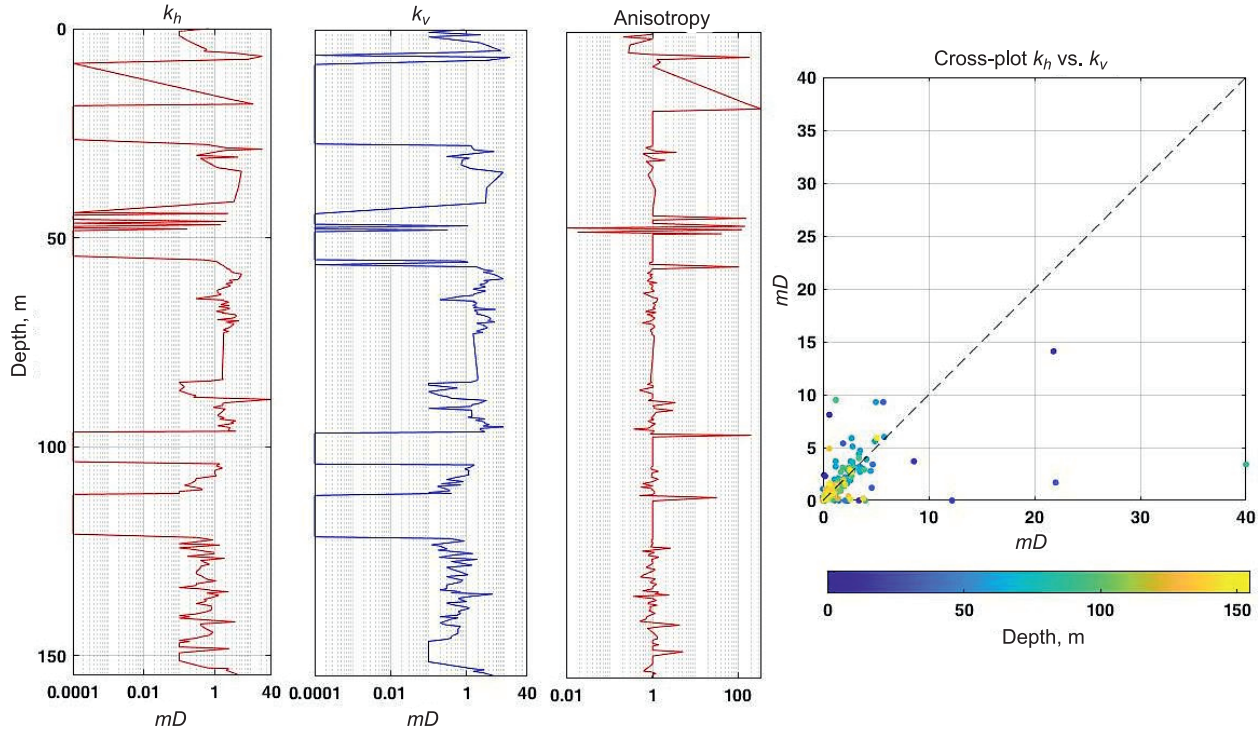

Fig. 8. k_h (track 1), k_v (track 2), *g* (track 3), and cross-plot k_h vs. k_v (track 4).

This study was supported by the Petrobras human resources program and by Northern Rio de Janeiro State University. We also thank the Brazilian Petroleum Agency (ANP) for the dataset and LR Senergy (2020) for the assignment of the Interactive Petrophysics software.

REFERENCES

Ahr, W.M., 2011. Geology of Carbonate Reservoirs: the Identification, Description, and Characterization of Hydrocarbon Reservoirs in Carbonate Rocks. Wiley, New Jersey.

Archie, G., 1942. The electrical resistivity log as an aid in determining some reservoir characteristics. Trans. AIME 146 (01), 54–62, SPE-942054-G, doi: 10.2118/942054-G.

Bruhn, C., Gomes, J., Lucchese, C., Jr., Johann, P., 2003. Campos Basin: reservoir characterization and management – historical overview and future challenges. Offshore Technology Conf., Houston, Tex., Paper OTC 15220, doi: 10.4043/15220-MS.

Burden, F., Winkler, D., 2008. Bayesian regularization of neural networks, in: Livingstone, D.J. (Eds.), Artificial Neural Networks. Methods in Molecular Biology, Vol. 458. Humana Press, pp. 23–42.

Doveton, J., 2014. Principles of Mathematical Petrophysics. Oxford University Press, Oxford.

Ellis, D., Singer, J., 2007. Well Logging for Earth Scientists, 2nd ed. Springer, Dordrecht.

Focke, J., Munn, D., 1987. Cementation exponents in Middle Eastern carbonate reservoirs. SPE Form. Eval. 2 (02), 155–167, doi: 10.2118/13735-PA.

Gartner, J., Suau, J., 1980. Fracture detection from well logs. The Log Analyst 21 (02), SPWLA-1980-vXXIn2a1.

Glover, P., 2009. What is the cementation exponent? A new interpretation. The Leading Edge 28 (1), 82–85, doi: 10.1190/1.3064150.

Glover, P., 2016. Archie's law – a reappraisal. Solid Earth 7 (4), 1157–1169, doi: 10.5194/se-7-1157-2016.

Hakimi, M., Shalaby, M., Abdullah, W., 2012. Application of well log analysis to assess the petrophysical parameters of the Lower Cretaceous Biyad Formation, East Shabowah Oilfields, Masila Basin, Yemen. WASJ 16 (9), 1227–1238.

Kennedy, M., 2015. Practical Petrophysics. Developments in Petroleum Science. Elsevier, Amsterdam, Vol. 62.

LR Senergy, 2020. Interactive Petrophysics, v. 4.3. Online User's Manual (http://www.lr-senergy.com/software/ip). Accessed 7 December 2020.

Lucia, F., 1983. Petrophysical parameters estimated from visual descriptions of carbonate rocks: a field classification of carbonate pore space. JPT 35 (3), 629–637, doi: 10.2118/10073-PA.

Luthi, S., 2001. Geological Well Logs: Their Use in Reservoir Modeling. Springer, Berlin.

Ohen, H., Enwere, P., Daltaban, S., 2002. The role of core analysis data in the systematic and detailed modeling of fractured carbonate reservoir petrophysical properties to reduce uncertainty in reservoir simulation. SCA 2002-49.

Okubo, J., Lykawka, R., Warren, L., Favoreto, J., Brito, D., 2015. Depositional, diagenetic, and stratigraphic aspects of Macaé Group carbonates (Albian): Example from an oilfield from Campos Basin. Braz. J. Geol. 45 (2), 243–258, doi: 10.1590/23174889201500020005.

Olive, D., 2017. Multiple linear regression, in: Linear Regression. Springer, pp. 17–83.

Petrobras, 2012. Oilfield B Report. Petrobras – UENF Agreement [in Portuguese].

Sahin, A., Ali, A., Saner, S., Menouar, H., 2007. Permeability anisotropy distributions in an upper Jurassic carbonate reservoir, eastern Saudi Arabia. J. Pet. Geol. 30 (2), 147–158, doi: 10.1111/j.1747-5457.2007.00147.x.

Schlumberger, 1989. Log Interpretation, Principles/Applications. Schlumberger Wireline and Testing, Sugar Land, Tx.

Schön, J., 2011. Physical Properties of Rocks: A Workbook. Handbook of Petroleum Exploration and Production. Vol. 8. Elsevier, Amsterdam.

Serra, O., Serra, L., 2004. Well Logging and Geology. SerraLog, Calvados.

Tiab, D., Donaldson, E., 2012. Petrophysics: Theory and Practice of Measuring Reservoir Rock and Fluid Transport Properties, 3rd ed. Gulf Publishing Company, Oxford.

Timur, T., 1968. An investigation of permeability, porosity, and residual water saturation relationships for sandstone reservoirs. The Log Analyst 9 (04), SPWLA-1968-vIXn4a2.

Wyllie, M., 1957. The Fundamentals of Electric Log Interpretation. Academic Press, New York.

Wyllie, M., Gregory, A., Gardner, L., 1956. Elastic wave velocities in heterogeneous and porous media. Geophysics 21 (1), 41–70, doi: 10.1190/1.1438217.